Pergamon

Scripta Materialia, Vol. 39, No. 10, pp. 1333–1338, 1998
Elsevier Science Ltd

1359-6462/98 $19.00 + .00

PII S1359-6462(98)00328-5

INTERFACIAL REACTIONS BETWEEN ZIRCONIA AND TITANIUM

Kun-Fung Lin and Chien-Cheng Lin
Department of Materials Science and Engineering, National Chiao Tung University, Hsinchu, Taiwan 300

(Received March 10, 1998)
(Accepted in revised form August 3, 1998)

Introduction

Titanium alloys have excellent properties such as high specific strength and good corrosion resistance. However, they are extremely reactive to ceramics at high temperatures, resulting in a chemical reaction affected-surface [1]. The interstitial elements (e.g., C, N, O, H) from the ceramic have a great tendency to enter into the titanium alloys and cause the deterioration of mechanical properties [2]. Economos and Kingery [3] found that titanium melt could penetrate along the grain boundaries of oxides, such as Al_2O_3, ZrO_2, and MgO, at 1800°C, leading to the alternation of these oxides. Ruh [4] indicated that the titanium could react with zirconia and up to 10 at% of Zr and O elements from ZrO_2 were retained in the solid solution of Ti, while the zirconia was transformed into oxygen deficient zirconia. Saha [5] also revealed that ZrO_{2-x} and α-Ti(O) were formed after Ti reacted with ZrO_2. However, the interfacial reactions between zirconia and titanium has not been fully elucidated to date.

In this study, the microstructure of the interface between zirconia and titanium has been investigated using an analytical transmission electron microscope with a dedicated energy dispersive spectrometer (TEM/EDS), and the mechanism of the interface reactions is also discussed.

Experimental Procedures

A commercially pure titanium powder (CP-Ti, 200 mesh, 99.8%) and several calcia partially stabilized ZrO_2 plates (~9 mm thick, 5 mol %CaO-ZrO_2) were loaded in a zirconia crucible (5C–ZrO_2), and then put in an electric resistance furnace. The chamber was evacuated to 10^{-4} torr and then backfilled with argon to atmospheric pressure. This cycle of evacuation and purge with argon was repeated at least twice. It took 30 minutes to raise the temperature from 100 to 1600°C and 5 minutes from 1600 to 1750°C, and then held at 1750°C for 7 minutes. During cooling, the temperature was lowered to 1600°C at the cooling rate of 30°C/min, to 1000°C at 50°C/min. Next, the specimen was cooled down to room temperature in furnace. The interface of zirconia and titanium was observed using an analytical TEM (JOEL JEM 2010) as well as a scanning electron microscope (JXA 6400). The cross-sectional TEM specimens perpendicular to the interface of zirconia and titanium were prepared by standard procedures of cutting, grinding, polishing, and ion milling. The quantitative composition analyses, with an error less than ± 5%, were carried out based on the principle of Cliff-Lorimer [6] by an energy dispersive spectrometer (EDS; Model ISIS 300) attached to the TEM.

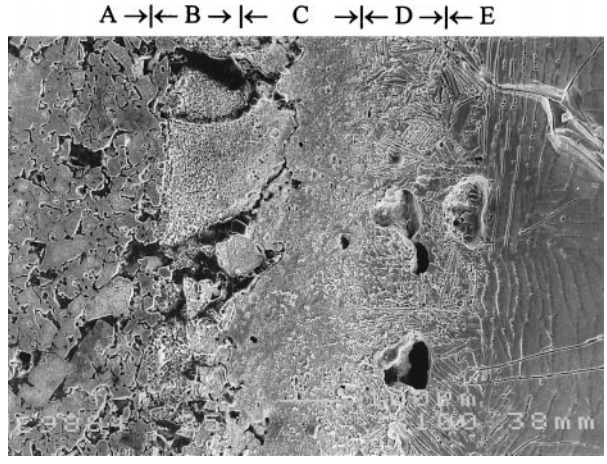

Figure 1. An SEM micrograph showing the interface between zirconia and titanium after reaction at 1750°C/7 min. Zone A: unaffected ZrO_2; Zone B: ZrO_{2-x} layer; Zone C: chemical reaction layer; Zone D: α-case; Zone E: unaffected Ti.

Results and Discussions

(a) SEM Analyses

Figure 1 displays an SEM micrograph showing the interface between zirconia and titanium after reaction at 1750°C/7 min. The unaffected ZrO_2 with a porous structure is located at the most left end, while the unaffected titanium is in the right end. At high temperatures, the liquid titanium infiltrated into zirconia through the open pores forming a thick chemical reaction zone (indicated as Zone C) at the interface. A layer of the oxygen deficient zirconia (ZrO_{2-x}) (indicated as Zone B) is to the left of this chemical reaction layer (Zone C). A change in the color of calcia partially stabilized zirconia (from light yellow to gray black) after reaction indicated oxygen deficiency caused by the extensive reduction of

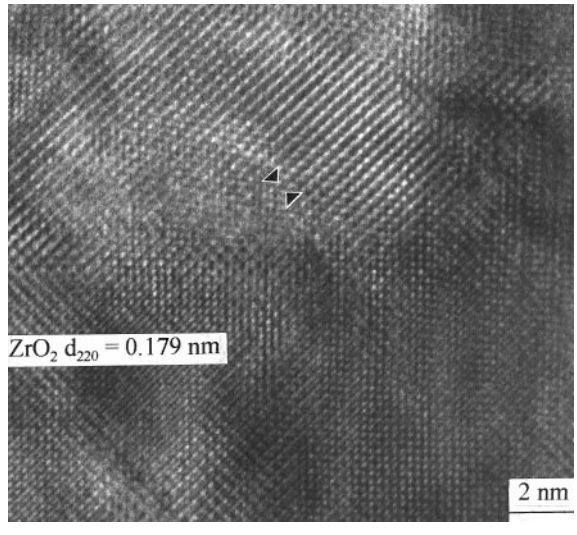

Figure 2. A high resolution TEM micrograph of the ZrO_2/TiO_2 interface.

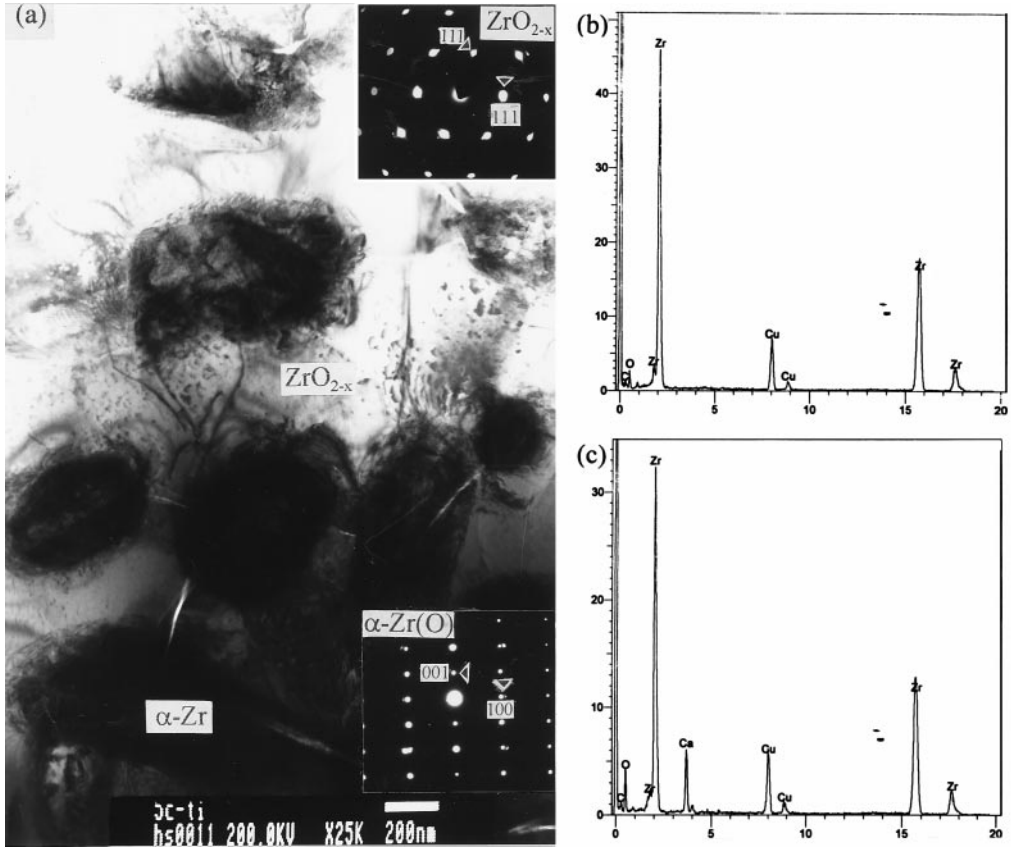

Figure 3. (a) A bright field image of α-Zr(O) and ZrO_{2-x}; (b) an EDS of α-Zr(O); (c) an EDS of ZrO_{2-x}.

ZrO_2 [7]. To the right side of the chemical reaction zone (Zone C) there exists a needle-like α-phase (indicated as Zone D). In addition, there were many micro-pores along the grain boundaries of this α-phase. This implies that zirconia lost oxygen and oxygen was dissolved in titanium, leading to the formation of α-titanium and small oxygen pores.

(b) TEM Observations

Formation of TiO_2. TiO_2 was observed in the chemical reaction zone (Zone C in Fig. 1). At high temperatures, oxygen was leached from ZrO_2 and dissolved in titanium melt. TiO_2 could be formed if the reaction between zirconia and titanium was extensive. Figure 2 presents a high resolution image of the ZrO_{2-x}/TiO_2 interface with (220) plane of ZrO_{2-x} being slightly misaligned with [101] plane of TiO_2. The phase diagram of ZrO_2-TiO_2 [8] indicates that a two-phase region of $ZrTiO_4$ and TiO_2 in the part of rich TiO_2. But $ZrTiO_4$ was not found in this study.

Formation of α-Zr(O). Figure 3(a) displays a bright field image of α-Zr(O) and ZrO_{2-x} (Zone B or Zone C in Fig. 1). Spherical α-Zr(O) particles were randomly distributed in ZrO_{2-x}. Inset in the lower right corner of Fig. 3(a) is the selected area diffraction pattern (SADP) of α-Zr, while ZrO_{2-x} (designated as primary ZrO_{2-x}) was identified to be a cubic phase. The EDS in Fig. 3(b) confirmed that the spherical particles were α-Zr with a limited solubility of oxygen (note that Cu peaks in the EDS

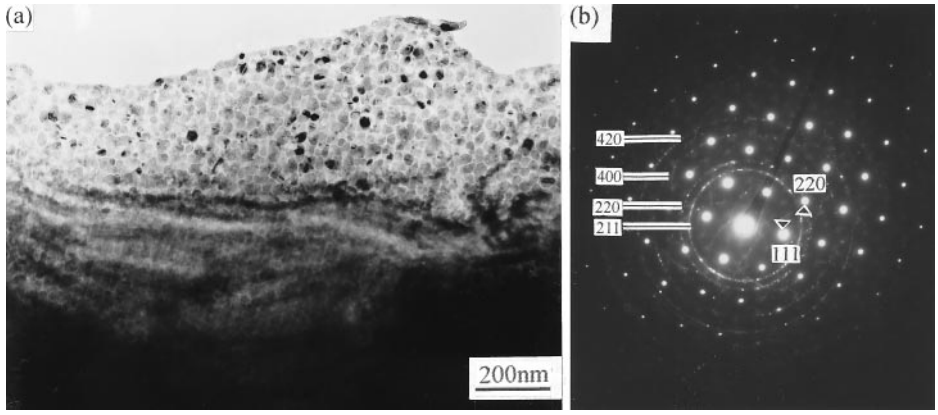

Figure 4. (a) A bright field image of secondary ZrO_{2-x} crystallites; (b) an SADP showing diffraction rings caused by the secondary ZrO_{2-x} crystallites in (a).

spectrum were caused by the contamination of the copper grip during ion milling.) Figure 3(c) depicts an EDS result of the cubic ZrO_{2-x}, showing that the cubic ZrO_{2-x} dissolved 12.79 at% Ca. It implies that Ca remained in ZrO_{2-x} and the ratio of CaO/ZrO_2 after the precipitation of α-Zr(O) from the primary ZrO_{2-x} became larger than that in the original 5C-ZrO_2.

Zr-O phase diagram [9] displayed a two phase region of α-Zr(O) and c-ZrO_{2-x} in a wide region (32.5 at%O-63.5 at%O) above the eutectoid temperature ($\approx$1525°C). Since x was around 0.3 in ZrO_{2-x} in this study, the equilibrium Zr/O ratio in ZrO_{2-x} decreased with decreasing temperature. ZrO_{2-x} could transform to the one with a higher oxygen content by the ex-solution of α-Zr(O) during cooling, and spherical α-Zr(O) simultaneously precipitated in the primary ZrO_{2-x}.

Formation of secondary ZrO_{2-x} crystallites. Nano-cystalline particles in Fig. 4(a) were identified to be cubic zirconia from the diffraction rings in Fig. 4(b). The O/Zr ratio of these cubic zirconia crystallites was determined to be close to 1.9 by the Cliff-Lorimer method. Note that the diffraction spots in Fig. 4(b) were caused by the untransformed primary ZrO_{2-x}.

The transformation of zirconia in this study can be described as follows: ZrO_2 was reduced to primary ZrO_{2-x} by titanium at high temperatures. Spherical proeutectoid α-Zr(O) would precipitate, while the O/Zr ratio of the primary ZrO_{2-x} increased. As the temperature decreased, secondary ZrO_{2-x} crystallites with the O/Zr ratio being close to 1.9 were crystallized.

Oxygen deficient zirconia was stabilized during the interfacial reactions. The lowest temperature for cubic oxygen deficient zirconia was 1525°C and, at low temperatures, the monoclinic oxygen deficient zirconia existed in a very limited range [10]. However, the cubic ZrO_{2-x} was found in present study. There might be two reasons for the stabilization of ZrO_{2-x}: One is that its particle size was smaller than the critical size for the t $\rightarrow$ m transformation, while the other is that the CaO content increased in the primary ZrO_{2-x}.

Precipitation of $CaZrO_3$. $CaZrO_3$ precipitated from the solid solution of primary ZrO_{2-x} as the ratio of CaO/ZrO_2 increased due to the ex-solution of α-Zr(O) (Zone C in Fig. 1). Figure 5(a) displays a TEM micrograph showing several oval $CaZrO_3$ embedded in α-Zr(O). The EDS result in Fig. 5(b) confirms the existence of $CaZrO_3$. Figure 5(c) depicts the EDS result of α-Zr(O), indicating that α-Zr(O) contained only Zr and O elements. The content of Ca in ZrO_{2-x} increased after α-Zr(O) was excluded from ZrO_{2-x}. At the eutectoid temperature of CaO–ZrO_2 (1140°C) [11], the solid solution of ZrO_{2-x} with more than 17 mol% CaO could decompose into tetragonal zirconia solid solution and two ordered phase (φ_1: $CaZr_4O_9$, and φ_2: $Ca_6Zr_{19}O_{44}$). However, the rates of decomposition to ordered phases are

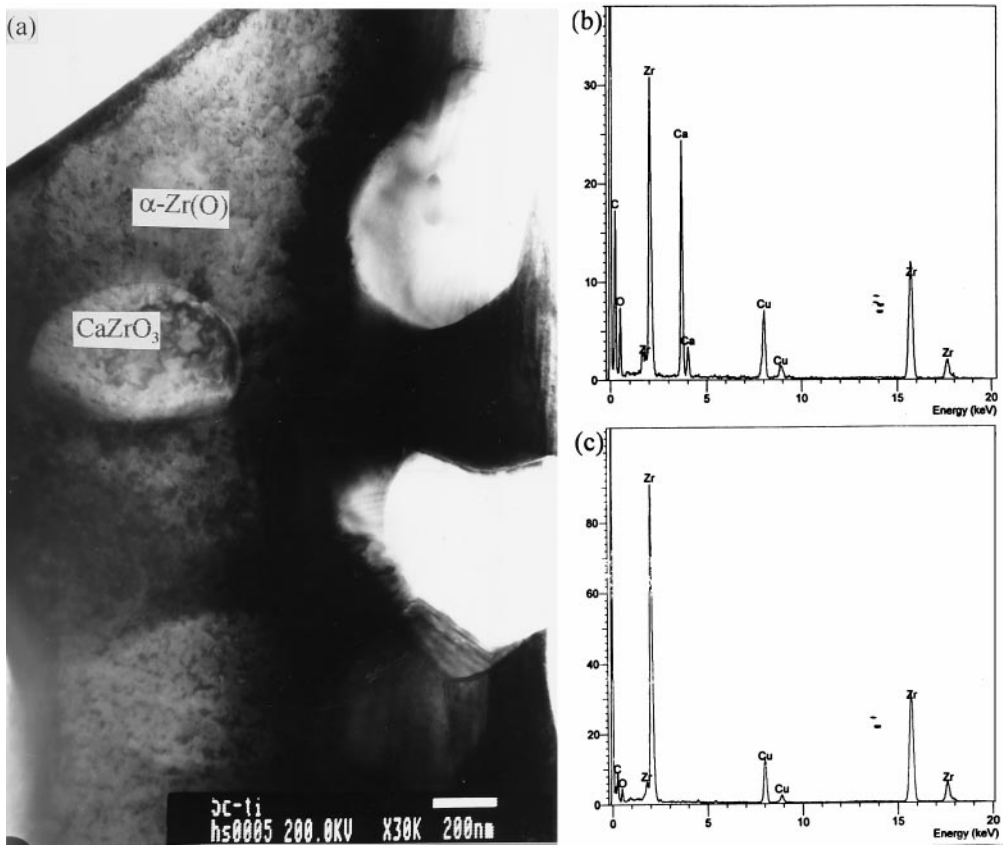

Figure 5. (a) A bright field image showing $CaZrO_3$ and α-Zr(O); (b) an EDS of $CaZrO_3$; (c) an EDS of α-Zr(O).

very slow at relatively low temperatures (<1400°C) [12]. Therefore, only $CaZrO_3$ precipitated, leaving α-Zr(O) to remain in the matrix.

Summary

Interfacial reactions between zirconia and titanium were proceeded by the infiltration of liquid titanium through the open pores of zirconia. During reaction, zirconia was reduced to oxygen-deficient zirconia (ZrO_{2-x}) and resulted in the liberation of oxygen. The dissolution of oxygen in titanium gave rise to the needle-like α-phase as well as TiO_2 in the reaction zone. The content of oxygen in ZrO_{2-x} increased because of the ex-solution of proeutectoid spherical particles α-Zr(O). On cooling, secondary ZrO_{2-x} crystallites with O/Zr $\approx$ 1.9 were found. Furthermore, the Ca content increased in the solid solution of ZrO_{2-x} that could induce the precipitation of $CaZrO_3$.

References

1. R. L Saha and K. T. Jacob, Def. Sci. J. 36, 121 (1986).
2. M. J. Donachie Jr., Titanium: A Technical Guide, p. 40, ASM International, Metals Park, OH (1988).
3. G. Economos and W. D. Kingery, J. Am. Ceram. Soc. 36, 403 (1953).

4. R. Ruh, J. Am. Ceram. Soc. 46, 301 (1963).
5. R. L. Saha, T. K. Nandy, R. D. K. Misra, and K. T. Jacob, Metal. Trans. 21B, 559 (1990).
6. G. Cliff and G. W. Lorimer, J. Microsc. 103, 203 (1975).
7. G. M. Ingo, J. Am. Ceram. Soc. 74, 381 (1991).
8. R. S. Roth, T. Negas, and L. P. Cook, Phase Diagrams for Ceramists, p. 169, American Ceramics Society, Columbus, OH (1981).
9. H. Baker, ASM Handbook, Alloy Phase Diagrams, vol. 3, p. 2.326 (1992).
10. R. J. Ackermann, S. P. Garg, and E. G. Rauh, J. Am. Ceram. Soc. 60, 341 (1977).
11. J. R. Hellmann, and V. S. Stubican, Mater. Res. Bull. 17, 459 (1982).
12. J. R. Hellmann and V. S. Stubican, J. Am. Ceram. Soc. 66, 260 (1983).